Journal of Materials Science and Engineering A 10 (5-6) (2020) 96-102
doi: 10.17265/2161-6213/2020.5-6.003

Influence of Cu_9Al_4 Phase on Nanomechanical Behavior of Cu-14Al-4Ni-*x*Ti Shape Memory Alloy Rapidly Solidified

Marlon Silva[1], Igor Santos[1], Marília Bortolotto[1], Nicole Araújo[1], Pedro Lima[1], Marcelo Nava[1] and Emmanuel Lima[2]

1. DATM, Federal Institute of Education, Science and Technology of Bahia—IFBA, Salvador-BA 40301-015, Brazil

2. Faculdade do Gama—FGA, Universityof Brasília—UnB, Gama-DF 72444-240, Brazil

Abstract: This paper aims to verify the Cu_9Al_4 phase influence on the nanomechanical behavior of the Cu-14Al-4Ni-*x*Ti alloy obtained by rapid solidification with addition of different amounts of Ti. Using the Scanning Electron Microscopy (SEM), Atomic Force Microscopy (AFM), Energy Dispersion Spectroscopy (EDS) and X-Ray Diffraction (XRD), it was possible to perform the samples' microstructural characterization. In addition, the reduction of the Cu_9Al_4 phase precipitation and the X-phase appearance were verified according to the increase of the titanium percentage added. The nanomechanical behavior was evaluated by nanoindentation tests, which showed a significant decrease of the elastic modules and an increase of the Poisson coefficient's according to the titanium amount. This research establishes that the reduction of Cu_9Al_4 phase implies on the increase of the capacity to dissipate energy. Therefore, the high damping capacity combined with the X-phase presence increases the super elasticity and the alloy ductility.

Key words: Cu-14Al-4Ni-*x*Ti, shape memory effect, microstructure, nanoindentation, superelasticity.

Nomenclature

E	elastic module obtained
Q	effective contact area
h_c	residual deformation value
K	indenter constant
E^*	simplified elastic module
E_i	elastic module of the indenter of type Berkovich
G	grain size ASTM
L	grain length (millimeters)
S	contact stiffness

Greek Letters

β'	adjustment constant for the indenter of type Berkovich
V	Poisson's ratio of the material
v_i	Poisson's ratio of the indenter of type Berkovich

1. Introduction

The properties of the shape memory alloy (SMA) are mostly related to the reverse martensitic transformations. This is characterized by the low energy and high mobility of the interfaces between the phases, martensitic and matrix, when the variations in temperature or stress application are too small [1].

The Cu-Al-Ni alloys have the same properties as the SMAs and present a good internal friction behavior [2].

However, due to the elastic anisotropy, there is a great susceptibility to the fragile intergranular fracture [3], where the multiple crack nucleation occurs in the contours of the grains provoked by the Cu_9Al_4 phase [4]. For this reason, it is impossible to apply it in industrial systems. Nevertheless, the low ductility can be improved by grain refinement through adding Ti and the rapid solidification process. This process can be achieved by applying high cooling rates (102-106 K/s) or imposing high levels of supercooling by minimizing or eliminating nucleating agents [5].

Corresponding author: Pedro Lima, PhD, professor, research fields: materials science, mechanical engineering.

The supercooling technique of a liquid alloy allows, through the high rates of heat extraction, obtaining materials with microstructures in a state of equilibrium, producing more stable structures than cooling slowly [6]. Besides that, the fast solidification process can also generate solid supersaturated solutions, metastable phases, structures with refined grains, which are also homogeneous without segregation and other amorphous structures [7].

2. Materials and Methods

The samples were fused by electric arc and supercooled by pressure difference in a copper mold at 20 °C, this process occurred under inertial atmosphere. The materials, which compose the alloys, were selected with a high purity level, weighed and subjected to a chemical stripping process in NaOH solution.

Three samples with different percentages of Ti (0.5, 0.6 and 0.7%) and one without Ti were obtained in ingots of 5 g each. After the smelting process, all samples were cut, polished and etched with a solution composed by 5 g $FeCl_3$, 100 mL H_2O and 50 mL HCl.

To determine the chemical composition, the technique of energy-dispersive spectroscope (EDS) (TESCAN, Czech Republic) was used. The microstructural characterization was accomplished by using SPM9700 atomic force microscope (AFM) (Shimadzu, Japan). The microstructure evolution was evaluated according to the amount of Ti added.

The phase determination was performed using XRD7000 X-Ray Diffraction (Shimadzu, Japan) subjecting the samples to a voltage of 40 kV and a current of 30 mA at a steady state 2θ and a rate of 1°/min between 30° and 120°.

The nanoindentation test was performed using the PB1000 (Nanovea, USA) with a diamond Berkovich type indenter applying a maximum load of 100 mN.

The method of Oliver and Pharr [8] allows determining accurately and experimentally the Young's modulus of the alloy, because this technique works with deformations close to the atomic scale and in specific fields of tension.

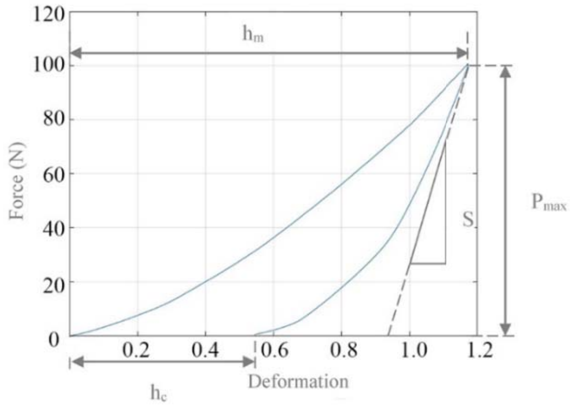

Fig. 1 Graphic representation of sample loading and unloading curves without T.

As shown in Fig. 1, the samples were subjected to a loading and unloading cycle, where h_c is the residual deformation value, h_m the maximum deformation and S is the contact stiffness.

The effective contact area Q, can be calculated by Eq. (1). K is the constant related to the characteristics of the indenter and is equal to 24.56.

$$Q = Kh_c^2 \tag{1}$$

Eq. (2) allows to calculating the simplified elastic modulus, where β' is an adjustment constant for the indenter of type Berkovich with the value of 1.05.

$$E^* = \frac{\sqrt{\pi}}{\beta'} \times \frac{S}{\sqrt{Q}} \tag{2}$$

The Poisson's ratio can be determined analytically through Eq. (3):

$$E = (1 - v^2)\left(\frac{1}{E^*} - \frac{1 - v_i^2}{E_i}\right)^{-1} \tag{3}$$

E corresponds to the elastic modulus obtained through the nanoindentation test and v corresponds to the Poisson's ratio of the analyzed material. v_i and E_i are respectively the Poisson's ratio and the elastic modulus of the indenter of type Berkovich. E_i is equal to 1,141Gpa and v_i is equal to 0.07 [9].

3. Results and Discussion

The analysis of the chemical composition based on the energy-dispersive spectroscope (EDS), corresponds approximately to the percentages attributed to the samples. These values are shown in Table 1.

The results of the X-ray diffraction (XRD) analysis of the samples according to the Ti percentage added are shown in Fig. 2. It was verified, that during the supercooling process the β phase decomposes on the eutectoid point $\beta \rightarrow \alpha + \gamma_2 + \beta_2$ [10], where α represents a solid solution which is rich in copper and has a face centered cubic structure, the β_2 represents a NiAl phase of body-centered, cubic structure and γ_2 represents a solid solution of the type Cu_9Al_4 with a simple cubic crystalline structure. The intermetallic γ_2 phase represents microstructural homogeneity and is bonded to Ni, which is present in the alloy.

The Cu-14Al-4Ni alloy presents the predominant γ_2 phase as a crystalline structure due to the decomposition of the β phase of polycrystalline character, which tends to increase the fragility of the alloy.

The diffraction analysis of the Cu-14Al-4Ni alloy revealed a structure rich in γ_2 phase (90.7%) and with presence of β_2 phase (9.3%). The γ_2 phase represents a typical martensitic structure (β'1; 30.19º-63.5º) [11]. However, there was no α phase in the Cu-14Al-4Ni alloy.

The Cu-14Al-4Ni-0.5Ti alloy presented, due to the action of the Ti, a crystalline structure rich in γ_2 phase (92.02%) and the X-phase composed of $CuNi_2Ti$ (4.98%).

However, for the Cu-14Al-4Ni-0.6Ti alloy, the amount of Ti that served as a refiner contributes to the reduction of the γ_2 phase (53.95%) and to the formation of the phases $CuNi_2Ti$ (41.65%) and $AlCu_2Ti$ (4.4%).

Table 1 Chemical composition of the samples obtained by the EDS.

	Alloying elements wt%			
	Cu	Al	Ni	Ti
0.0% Ti	80.99-81.17	15.22-15.30	3.61-3.67	-
0.5% Ti	81.53-81.67	14.66-14.74	3.64-3.76	0.54-0.58
0.6% Ti	82.82-82.90	13.40-13.46	3.67-3.75	0.57-0.59
0.7% Ti	80.90-80.92	14.60-14.68	3.72-3.84	0.65-0.69

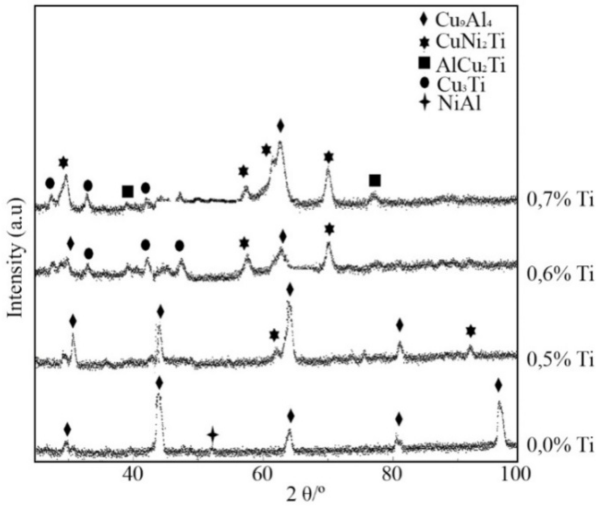

Fig. 2 Diffractograms of the alloys after the heat treatment of betatization.

Table 2 Percentages of the present phases in the alloys by XRD.

	Alloying phases wt%				
	Cu_9Al_4	NiAl	$CuNi_2Ti$	$AlCu_2Ti$	Cu_3Ti
0.0%Ti	90.70	9.30	-	-	-
0.5%Ti	95.02	-	4.98	-	-
0.6%Ti	53.90	-	41.65	4.40	-
0.7%Ti	38.70	-	49.35	6.31	5.63

The diffraction analysis of the Cu-14Al-4Ni-0.7Ti alloy showed the beneficial effect of the 0.7% Ti content related to the reduction of the amount of the Cu_9Al_4 fragile phase. In addition, this amount of Ti contributes to the increase of the $CuNi_2Ti$ and $AlCu_2Ti$ phases. However, this Ti content also provided the formation of 5.6% of a typical martensitic structure, ordered by Cu_3Ti which is named X-phase [12].

Table 2 shows the arrangement of the present phases in each alloy, as well as the percentage in weight (wt%) relating to each phase. It is possible to notice a considerable reduction of the γ_2 phase according to the increase of the Ti content (0.6% and 0.7%), except for 0.5% Ti alloy. For the Cu-14Al-4Ni-0.6Ti and Cu-14Al-4Ni-0.7Ti alloys, the formation of the $AlCu_2Ti$ alloy reduces the concentration of Ti in the matrix. It was noticed that the amount of the Cu_9Al_4 phase decreased with the increasing of Ti. Nevertheless, the precipitation of the γ_2 phase can not be completely suppressed. This would make the casting process instable due to the increase of the solidification rate [12].

The images obtained by AFM, shown in Figs. 3a-3d, illustrate the fine needle structures, which are typical of a martensitic structure, in the alloy with and without adding Ti. These structures are characteristic of the Cu_9Al_4 phase. The presence of this phase in the alloys can be confirmed through the diffractometric analyses.

In addition to the fine and long needle structure typical of martensitic structures formed after the heat treatment, the Cu-14Al-4Ni sample also showed fine grained contours. The Cu-14Al-4Ni-0.5Ti sample presented thicker and more visible grain contours compared to the sample without the Ti, which may be related to the higher percentage of the γ_2 phase in this alloy.

Figs. 4a-4c also show the X-phases, indicated by the arrows, of the samples obtained by EDS (backscattered electrons). These micrographs confirm the presence of globular particles referring to the X-phase, rich in Ti.

According to the ASTM E112 [13], the grain size can be measured and calculated through Eq. (4).

$$G = -3{,}2877 - [6{,}6439 \times \log(Lmm)] \quad (4)$$

The Hyen Intercept method was applied because it offers a greater reliability for the determination of non-equiaxed grains. G is the ASTM grain size and L is the measured grain length in millimeters. The grains were measured directly using AFM. The located average values were inserted into Eq. (4) and the results are shown in Fig. 5.

It was possible to verify the beneficial effect of the increase of the Ti in the Cu-14Al-4Ni alloy subjected to supercooling, betatization and quenching in regard to the grain size reduction. This effect implies improvements in mechanical properties due to the fragility reduction. It can be noticed, that the increase of the percentage of Ti also implies lower grain size variation as shown in Fig. 6. This fact can be justified by the conjunct action of the Ti added and the process of the rapid solidification, which gives the material a more refined granolumetry.

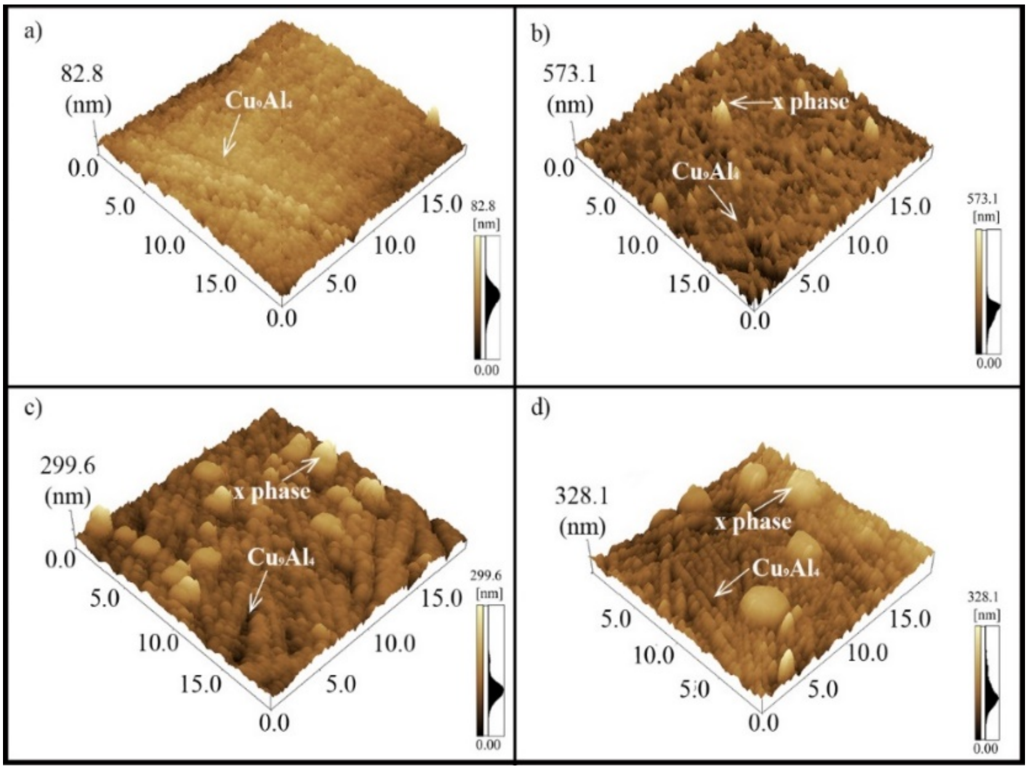

Fig. 3 Martensitic structures Cu_9Al_4 and x phase by AFM: (a) 0.0 Ti, (b) 0.5 Ti, (c) 0.6 Ti, (d) 0.7 Ti.

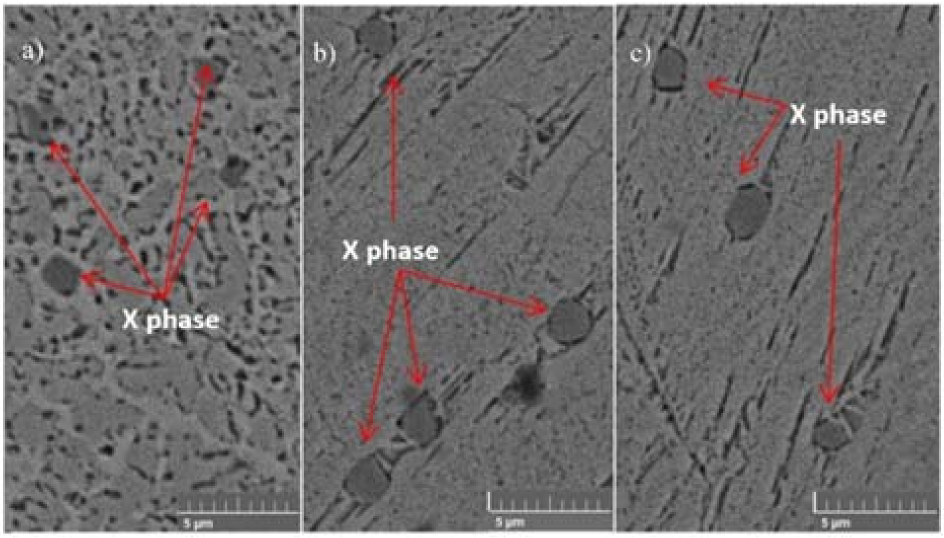

Fig. 4 X phase by EDS: (a) 0.5 Ti, (b) 0.6 Ti, (c) 0.7 Ti.

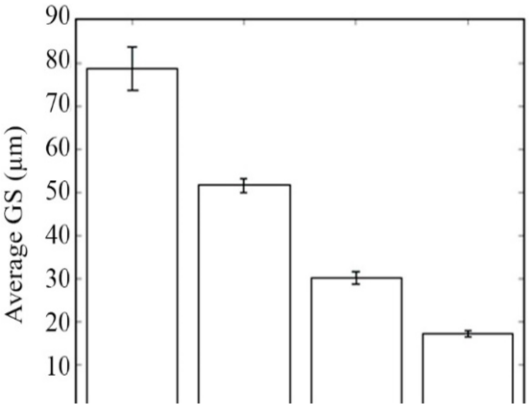

Fig. 5 Absolute grain size measure through AFM.

The Vickers nanoindentation analyses were performed in different regions of the cross section of all samples.

Through this technique it was possible to obtain the average of the HV hardness (kgf/mm^2) and the average of the Young's Modulus in GPa. Fig. 7 presents the relationship between the variation of the nanomechanical behavior, the elastic modulus and the nanohardness values of each sample under the influence of different Ti amounts.

The Poisson coefficients and the applied energy on the elastic and plastic deformation were obtained algebraically in Joule. It is known, that the elastic modulus is the stiffness of a material when it is subjected to an elastic deformation. However, on atomic scale the elastic deformation is manifested as small changes in the interatomic spaces and in the stretching of the interatomic bonds.

The increase of the Ti content (0.5% to 0.7%) caused a reduction of the separation resistance of the adjacent atoms in the interatomic bond strength. The elastic modulus of the alloy of the Cu-14Al-4Ni system can vary between 23 GPa and 235 GPa [14].

Fig. 8 shows the nanohardness analysis under the loading and unloading curves. The internal area of each graphic is numerically equal to plastic energy and is related to mechanical hysteresis. The area below the discharge curve is numerically equal to the elastic energy and can be associated with the resilience and damping capacity of the material.

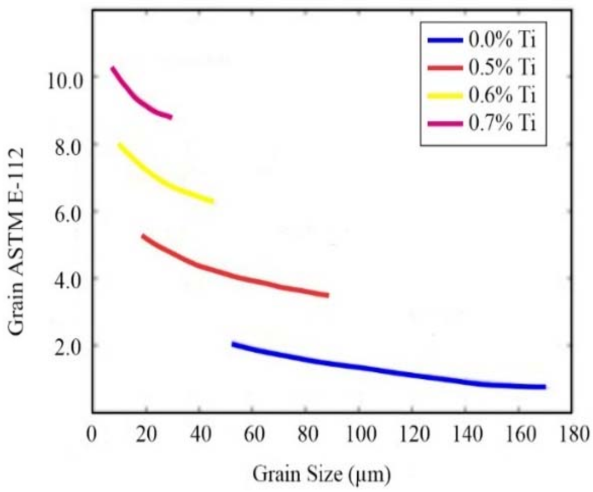

Fig. 6 Grain size ASTM (*G*) obtained by Eq. (4).

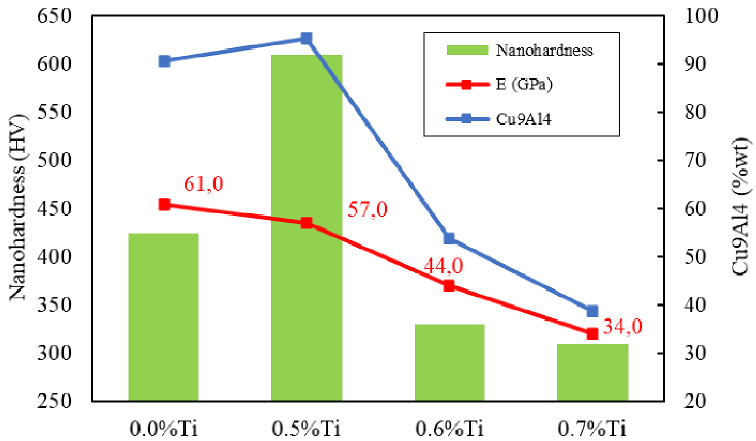

Fig. 7 Relationship between the percentage of the Cu_9Al_4 phase and the nanoindentation level and Young's Modulus.

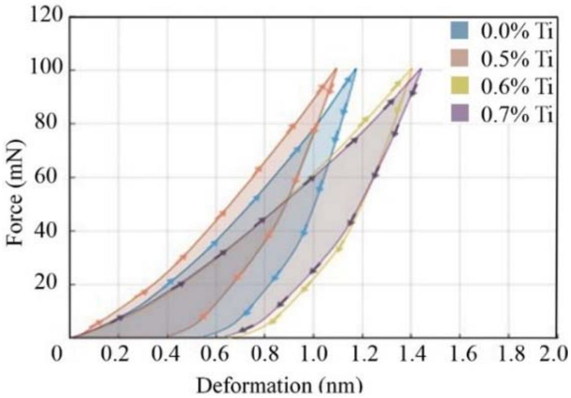

Fig. 8 Nanohardness under the loading and unloading curves.

4. Conclusions

For this research, concerning the crystalline structure of the alloys, the adopted manufacturing process suppresses the *α* phase precipitation, which is an intermetallic phase with high hardness and rich in copper. The addition of different amounts of Ti supports the reduction and homogenization of the grain size variation. Therefore, Ti is a grain refiner of the Cu-14Al-4Ni alloys.

The microstructure of the samples, evaluated by the atomic force microscopy (AFM), converged with the literature concerning the presence of the X-phase in the samples with Ti.

The amount of Cu_9Al_4 phase defines the nanomechanical behavior of alloys. The sample with a higher percentage of the Cu_9Al_4 phase consequently has a higher nanohardness and a lower energy dissipation capacity. The decrease in the quantity of the Cu_9Al_4 phase interferes with the reduction of the elastic modulus of the alloys and leads to the increase of the Poisson coefficient.

Furthermore, the presence of X-phases contributes to the super elasticity of the alloys and also to an increase in the energy dissipation capacity.

Acknowledgments

The authors would like to thank the Federal Institute of Science and Technology of Bahia, the University of São Paulo and the University of Brasilia for all the support to carry out this research.

References

[1] Otsuka, K., and Wayman, C. M. 1999. "Characteristics of Shape Memory Alloys." *Shape Memory Materials*, 149-83.

[2] Van Humbeeck, J., and Stalmans, R. 1999. "Characteristics of Shape Memory Alloys." In *Shape Memory Materials*, edited by Otsuka, K., and Wayman, C. M.

[3] Sobrero, C. E., Bolmaro, R., Malarría, J., Ochin, P., and Portier, R. 2008. "Texture in Cu-Based Shape Memory Strips Obtained by Twin Roll Casting." *Materials Science and Engineering A* 481-482: 688-92.

[4] Lojen, G., Anzel, I., Keneissl, A., Krizman, A., Unterweger, E., Kosec, B., and Bizjak, M. 2005. "Microstructure of Rapidly Solidified Cu-Al-Ni Shape Memory Alloy Ribbons." *Journal of Materials Processing Technology*, 220-9.

[5] Herlach, D. M. 1994. "Non-equilibrium Solidification of Undercooled Metallic Melts." *Materials Science and*

Engeneering R12: 177-272.

[6] Srivantsan, T. S., et al., eds. *Rapid Solidification Technology: An Engineering Guide*. Lancaster, PA: Technomic Publishing Co. Inc. p. 71.

[7] Jones, H. 2001. "A Perspective on the Development of Rapid Solidification and Nanoequilibrium Processing and Its Future." *Materials Science and Engineering A* 304-306: 11-9.

[8] Oliver, W. C., and Pharr, G. M. 1992. "An Improved Technique for Determining Hardness and Elastic Modulus Using Load and Displacement Sensing Indentation Experiments." *J. Mater. Res*. 7: 1564-83.

[9] Janakiraman, N. A. 2010. "Indentation Analysis of Elastic and Plastic Deformation of Precursor-Derived Si-C-N Ceramics." *Journal of the European Ceramic Society* 30: 775-85.

[10] Sedlák, P., Seiner, H., Landa, M., Novák, V., Sittner, P., and Mañosa, L. 2005. "Elastic Constants of BCC Austenite and 2H Orthorhombic Martensite in CuAlNi Shape Memory Alloy." *Acta Materialia* 53: 3643-61.

[11] Matlakhova, L. A., Pereira, E. C., Matlakhov, A. N., Monteiro, S. N., and Rodriguez, R. J. S. 2015. "Stress Assisted Thermal Cycling Treatment of a Monocrystalline Cu-Al-Ni Alloy." *Materials Science Research Journal* 5: 31-50.

[12] Lima, P. C. 2018. "Study of the Effect of Titanium Addition in Grains Size, as Processing Temperatures Phase and Elastic Module of Cu-14Al-4Ni Alloy with Arc Fusion Memory Effect and Rapid Vacuum Solidification." Ph.D. thesis, Department of Mechanical Engineering, Faculty of Technology, University of Brasilia – Brazil.

[13] Wang, Z., Xue-Feng, L., and Jian-Xin, X. 2011. "Effects of Solidification Parameters on Microstructure and Mechanical Properties of Continuous Columnar-Grained Cu-Al-Ni Alloy." *Progress in Natural Science: Materials International* 21 (5): 368-74.

[14] ASTM E-112. 1996. *Standard Test Method for Determining Avarage Grain Size*.

[15] Otsuka, K., and Waiman, C. M. 1998. *Shape Memory Materials.* 1st ed. Cambridge: Cambridge University Press.